*Submitted to Experimental Thermal and Fluid Science*

# EXPERIMENTAL STUDY OF MECHANICAL AND THERMAL NON-EQUILIBRIUM EFFECTS ON CHOKING FLOW AT LOW PRESSURE

H. J. Yoon*, M. Ishii, and S. T. Revankar
School of Nuclear Engineering, Purdue University
West Lafayette, IN 47906

W. Wang
US Nuclear Regulatory Commission
11555 Rockville Pike, Rockville, MD 20852

*Corresponding author.
Phone: 1-765-496-3902
Fax: 1-765-494-9570
E-mail: hyoon@purdue.edu

**ABSTRACT**

The mechanical and thermal non-equilibrium effects on adiabatic air-water and subcooled water choking flow were studied experimentally for pressure up to 1 MPa. A typical nozzle and orifice were used as the choking flow section to evaluate the degree of non-equilibrium due to geometrical effects. The slip ratio, which is a key parameter to express the mechanical non-equilibrium, was directly measured upstream of the choking section for the air-water test. The experimental results showed that the slip ratio increased with the quality. The slip ratio value at low pressure (<345kPa) was higher than the slip ratio at the high pressure (>517kPa) for the same flow quality. The measured choking mass flux for the nozzle was higher than the orifice at low flow quality (<0.05). This indicated that the throat geometry affected the choking mass flux at the low quality region, even though there was no difference in the slip ratio at the upstream of the choking plane. The thermal non-equilibrium effect was very strong at low pressure, however, no major influence of the geometry on this effect was observed in the subcooled water condition. The test data for subcooled water showed moderate decrease of choking mass flux with decreasing subcooling.
**KEYWORD** : Air-water Choking Flow, Subcooled Water Choking Flow, Mechanical Non-equilibrium, Thermal Non-equilibrium, Slip Ratio

## 1. INTRODUCTION

The choking flow is an important phenomenon that occurs in wide range of industrial system. This phenomenon is very important in the safety assessment of a water cooled nuclear power plant. In the event of loss of coolant accident (LOCA), the choking flow determine the water inventory of the reactor vessel, and the integrity of core eventually depends upon the choking flow [1]. Therefore, analytical description and prediction of choking flow rate plays an important role in the design of the engineered safeguards and

operation of the nuclear power plant. The serious study of two-phase flow was started as early as 1892 by Sauvage [2]. Rateau [3] showed the existence of choking flow in the boiling water flow through a nozzle, where the choking condition was obtained by reducing the back pressure. Rateau [3] also performed quality calculation method for the discharged saturated water through nozzle based on isentropic expansion. In the early choking flow model mechanical and thermodynamic equilibrium between gas and liquid phases were commonly assumed. This model is called the homogeneous equilibrium model. In this model, the two phases are in equilibrium with equal velocities and temperatures. The thermodynamic properties are used from the steam table, and the equation of state is used. However, this assumption is valid only for some ideal conditions such as for a long pipe where there is sufficient time for equilibrium to be achieved and when the flow pattern provides sufficient interphase forces to suppress significant relative motion.

The prediction of two-phase choking flow at low pressure is much more difficult than at relatively higher pressure (>1MPa). This is due to the large density ratio and relatively large thermal and mechanical non-equilibrium between the phases at low pressure. For low pressure blow down or choking flow, currently available models are not reliable and satisfactory. In view of these, choking flow tests were conducted to systematically investigate the effects of mechanical and thermal non-equilibrium on the two-phase choking flow in a pipe at low pressure. This type of systematic studies has never been performed before, therefore, no clear understanding of these effects has been attained prior to this research. Experimental study was conducted in a special test section with several in-line instruments for pressure up to 1 MPa.

## 2. CHOKING FLOW MODELS

The ultimate goal of the experiment is to supply the data basis in development of a model or model validation. Therefore, it is important to understand the existing choking flow models. Generally the choking flow models are classified as homogeneous equilibrium, homogeneous non-equilibrium, non-homogeneous equilibrium, and non-homogeneous non-equilibrium model.

### 2.1 Homogeneous Equilibrium Model

The homogeneous equilibrium model [4] is based on the assumptions of no slip, thermal equilibrium between phases, isentropic expansion and equation of state in the steam table. Thermal equilibrium means that the pressure and temperature of liquid and vapor are equal and are linked by the saturation curve.

The choking flow rate predicted from these assumptions is

$$G_c = \frac{\left\{2\left[h_o - (1-x_E)h_{fE} - x_E h_{gE}\right]\right\}^{1/2}}{\frac{(1-x_E)}{\rho_f} + \frac{x}{\rho_g}}. \qquad (1)$$

The choking mass flux can be reached by decreasing the downstream pressure until the flow rate reaches the maximum value. Beyond this, any back pressure reduction will not change the discharge flow rate because of the pressure singularity at the choking flow point. As can be noticed in equation (1), the choking mass flux in the homogeneous equilibrium model depends not on the break geometry or pipe length but on the upstream thermodynamic condition.

A feature of the homogeneous equilibrium model is adherence of the fluid properties along the saturation condition. In reality, the liquid can be superheated in order to nucleate

near the wall during the depressurization process. If the single-phase liquid velocity is high enough, the choking flow may occur at the outlet of the pipe with the nucleation of the first bubble. If the coolant temperature is low and nucleation is suppressed by non-equilibrium phenomena, then it might be required to consider the transition from single-phase to two-phase choking flow during the early stage of a blowdown in a LOCA analysis of a nuclear reactor [5]. The homogeneous equilibrium model showed good agreement with the Marviken critical flow data for subcooled stagnation condition and long pipe condition (L/D>1.5) [6]. However, in general, the homogeneous equilibrium model is not highly accurate for the subcooled liquid stagnation state [1,7]. The homogeneous equilibrium model can overestimate the choking flow rate when the break is large, and has rapid depressurization. However, according to results of Darby [8], the homogeneous equilibrium model underestimated the choking flow rate in short pipe. The homogeneous equilibrium model is applicable for the long pipe because this model is based on the no slip velocity, and there is sufficient time to establish the mechanical equilibrium in the long pipe. Since the homogeneous equilibrium model overestimates the mixture density in case of large break, it predicts more liquid discharge through the break.

Another approach of the homogeneous equilibrium model is Omega method. The analytical solution using this method was first proposed by Epstein et al. [9] for the steam-water mixture, and generalized by Leung [10] for any flashing two-phase mixture. They introduced the approximate equation of state which is given by

$$\frac{v}{v_{fo}} = \omega\left(\frac{P_s}{P} - 1\right) + 1, \tag{2}$$

where ω is given as

$$\omega = \frac{x_o v_{fgo}}{v_o} + \frac{c_{fo} T_o P_o}{v_o}\left(\frac{v_{fgo}}{h_{fgo}}\right)^2 \approx \alpha_o + \rho_o c_{fo} T_o P_o \left(\frac{v_{fgo}}{h_{fgo}}\right)^2 . \quad (3)$$

Based on these parameters, the expression for the normalized mass flux from momentum equation is

$$G^* = \frac{\left\{-2\left[\omega \ln \eta_1 + (1-\eta_1)(\omega - 1)\right]\right\}^{1/2}}{\omega\left(\frac{1}{\eta_1} - 1\right) + 1}, \quad (4)$$

where $\eta_1$ is the pressure ratio at the inlet. The choked mass flux based on equation (4) is given by [11]

$$G_c = \eta_c \left(\frac{P_o \rho_{fo}}{\omega \eta_s}\right)^{1/2}, \quad (5)$$

where subscripts, c and s refer to choking and saturation, respectively.

2.2 Homogeneous Non-equilibrium Model

Thermal non-equilibrium implies that there is a temperature difference between the phases. Thermal non-equilibrium is believed to be one of the major causes of the discrepancy between model predictions and experimental results, especially if subcooled fluid enters the choking section or the choking section is very short. According to the review presented by Abdollahian et al. [6] and Saha [12], one particular type of choking flow has escaped full understanding to date, even though a number of theoretical and experimental studies of choking flow have been reported. It occurs with a subcooled upstream condition that often

leads to significant non-equilibrium thermodynamic conditions at the choking section. At the choking section the liquid is superheated beyond the saturation temperature. This non-equilibrium effect is generated because the two-phase fluid depressurization rate may be faster than the thermal exchange rate between two phases [13]. This phenomenon occurs in the short choking section configuration. This metastable condition has been difficult to predict and is sensitive to the specific geometric characteristics of the break. This is because the local nucleation depends on the surface configuration, and liquid superheat and the bubble nucleation affects the relative motion between phases.

Actually, thermal non-equilibrium is related to the bubble nucleation. This was proven by several researchers using a delay time for nucleation time of order of 1ms [14,15]. Fauske (1985) showed a good agreement using the "relaxation length" by comparing with other data. This "relaxation time" or "relaxation length" corresponds to the super heat of 2-3 $^{o}$C.

Henry & Fauske [16] tried to account for the thermal non-equilibrium effect by introducing an empirical parameter, which represented the deviation from the homogeneous equilibrium model. This model assumed the phase separation at the entrance and neglected the friction loss. It is directly proportional to the difference between the exit qualities. In their model, the simplified choking mass flux is given as,

$$G_c^2 = \left[ \frac{x_o v_g}{nP} + \left(v_g - v_{fo}\right) \left\{ \frac{(1-x_o)N}{s_{gE} - s_{fE}} \frac{ds_{fE}}{dP} - \frac{x_o c_{pg}\left(1/n - 1/\gamma\right)}{P\left(s_{go} - s_{fo}\right)} \right\} \right]_t^{-1}, \qquad (6)$$

where n is polytropic exponent and N is an experimental parameter.

If N is unity, the prediction of above equation converges close to that of the homogeneous equilibrium model, and if N is zero it gives the homogeneous frozen model

where no phase change takes place. Therefore, the quantity N describes the degree of the non-equilibrium phase change occurring at the throat between two limiting conditions. However, Abdollahian et al. [6] pointed out that the Henry-Fauske model in the subcooled flow regime overpredicted the Marviken data [17].

Shrock et al. [15] developed a two-step model. Initially "frozen" flow (constant quality) is assumed until the pressure drops by a certain amount below the saturation pressure. At that point sudden equilibrium is achieved, and downstream from this point, again the frozen flow occurs. It was stated by the authors that the model did not represent the real physical behavior, however they claimed that there was no satisfactory means to predict the number and size of microbubble in the liquid triggering the nucleation process. Schrock et al. [1] pointed out that the choking model which considered the thermal non-equilibrium should include the physics of the nucleation process and the bubble growth.

Levy et al. [18] developed a simplified homogeneous non-equilibrium flashing model. When there is a rapid pressure decrease along the flow direction, this model may be applicable. This model assumed that water should be superheated at a given local pressure before liquid flashed into steam and enough vapor would be generated to reduce the water superheat. In addition, the flow was assumed to be homogeneous. Finally, an isentropic process was used to calculate the non-equilibrium quality and choking flow rate. This model was compared with the data of Reocreux [19] and Zimmer et al. [20]. For those two data sets, this model's prediction was reasonable. A good agreement was also obtained with the large scale Marvinken tests [17] and many other small scale experiments [21,22]. However, the model may not properly account for the impact of depressurization rate upon non-equilibrium conditions. In addition, it underpredicts small scale tests at high pressures when the contraction zone is not followed by a constant cross-section length.

Finally, there is the frozen model as it is referred previously. This model is the limiting case of the homogeneous non-equilibrium model and it is based on the assumption of no heat and mass transfer between phases. By using the isentropic expansion for the vapor phase, the choking flow rate can be calculated from the gas dynamic principle. Lenzing et al. [23] used the homogeneous frozen flow model by introducing the two-phase discharge coefficient for the non-flashing two-component flow and Henry and Fauske model by using the two-phase discharge coefficient for the flashing one-component flow.

### 2.3 Non-homogeneous Equilibrium Model

The early model of the non-homogeneous equilibrium model derived by Moody [24] is an extension of the homogeneous equilibrium model, by allowing different vapor and liquid velocities. A slip ratio, S, defined as the velocity ratio between the vapor and liquid, is considered and treated as a variable which is determined by the condition of maximum kinetic energy flux at the exit. This category of models is called "slip flow model". The slip between two phases allows the gas phase to be discharged with the higher velocity than liquid phase and this is more realistic approach than the homogeneous flow assumption [7]. In Moody model both phases are at the same static pressure and in local equilibrium at entrance and the exit. The two-phase flow pattern at exit is annular flow without entrainment. The exit velocities of each phase are uniform. Moody model gives the local slip ratio of $S = V_g / V_f = \left(\rho_f / \rho_g\right)^{1/3}$ to get a maximum two-phase kinetic energy flow, whereas Fauske [25] obtains the slip ratio as $S = V_g / V_f = \left(\rho_f / \rho_g\right)^{1/2}$ by minimizing the momentum flow rate. Fauske [26] emphasized the importance of the mechanical non-equilibrium in terms of the slip. According to Fauske [26], the slip is generated due to the density ratio between two phases and, therefore, light phase is easily accelerated by means of pressure difference between the upstream and choking section. The friction between the phases and droplet

caused by the liquid entrainment reduces the relative velocity between two phases. For the saturated or subcooled water flow, the accelerative force establishes the pressure gradient and the vapor is generated. This results in the existence of different velocities between two phases, with the vapor velocity faster than the liquid. However, Fauske showed that the slip is independent of the quality using the results of Marchaterre and Patric [27], and the effect of slip ratio decreased with pressure increase. According to Fauske, the superficial velocity in choking condition is much high, therefore, it is reasonable that the slip ratio is not affected by the quality. Based on the non-homogeneous equilibrium assumption, Fauske [26] derived the choking relationship as follows

$$G_c = \left[ -S / \left[ \begin{array}{l} \left\{ (1-x+Sx)x \right\} \dfrac{dv_g}{dP} + \left\{ v_g \left(1+2Sx-2x\right) + v_f \left(2xS-2S-2xS^2+S^2\right) \right\} \dfrac{dx}{dP} \\ + \left\{ S\left[1+x(S-2)-x^2(S-1)\right] \right\} \dfrac{dv_f}{dP} \end{array} \right] \right]^{1/2} . \qquad (7)$$

However, the weak point of these two models is that they are derived based on the ideal flow patterns, annular or separated flow. Furthermore, they are based on the energy or momentum maximization or minimization assumption which has no theoretical basis. Furthermore, the slip ratio is not independent of the quality. Cruver et al. [28] pointed out the problem in the assumptions of Fauske's model, where it is assumed that the pressure gradient at the choking point is a finite maximum. However, according to Cruver et al. [28], $\partial v_m/\partial S$ is a minimum, not a maximum because $\partial^2 v_m/\partial S^2 = 2x(1-x)v_g/S^3$ is always positive, and the finite maximum for dP/dz does not exist.

## 2.4 Non-homogeneous Non-equilibrium Model

In the two-fluid model, it is possible to consider the mechanical non-equilibrium and the thermal non-equilibrium simultaneously through proper constitutive relations for interfacial transfer rates.

In this approach, a separate set of conservation equations is used for each phase as shown by Bouré [29] and Ishii [30]. Therefore, these equations have to contain terms describing heat, mass and momentum transfer between the phases. These constitutive relations are not very accurate in the present state-of the art, particularly under the choking flow conditions where very large convective acceleration and depressurization take place. Thus simplification of the above equations and often quite arbitrary assumptions are introduced to overcome the lack of knowledge. The separate flow model is easy to visualize the mechanical non-equilibrium and thermal non-equilibrium between phases, however, the actual geometry of the interface can be quite different from this flow due to wall nucleation and flashing.

Existing interfacial exchange models were described by Trapp and Ransom [31], where calculation procedure and the numerical implementation of the choked flow criterion were discussed. Possible weaknesses of their model are the modeling of non-equilibrium mass and heat transfer terms, thermal resistance to heat flux, virtual mass coefficient, and the use of derivatives of the equations of state in thermal equilibrium. This implies that the interfacial momentum and energy in highly non-equilibrium flow may not be accurately modeled by the conventional models, particularly due to the significant nucleation at the wall which is difficult to predict.

Richter [32] developed a separated flow model to calculate the choking flow rate for the steam-water mixture. Generally, the separate flow model requires several correlations for the unknown parameters. The Richter model considered mechanical and thermal non-

equilibrium in one approach. This model assumed steady state, one dimensional, non-homogeneous flow, and the heat transfer between phases limited mass transfer. The frictional pressure drop was not neglected for the long pipe case.

The result in model shows that the slip ratio in the bubbly flow regime is one. However, if the evaporation in expanding bubbly flow was limited by heat transfer, the small velocity difference played an important role in the heat transfer mechanism. That implies that the mechanical non-equilibrium affects the thermal non-equilibrium. For the churn-turbulent flow regime, the thermal non-equilibrium was negligible and the mechanical non-equilibrium was dominant in this flow regime. Although Richter's result was very interesting, the results depended on the chosen correlation, and it was questionable whether it might be applied to the low pressure. According to the review of Abdollahian et al. [6], this model was the most successful in predicting the entire region of the Marviken data.

## 3. EXPERIMENTAL FACILITY

The critical flow experiments were performed using PUMA (Purdue University Multidimensional integral test Assembly) facility of PURDUE University. The PUMA test facility was originally designed as a scaled integral model of the General Electric Simplified Boiling Water Reactor (SBWR) [33,34]

Reactor pressure vessel (RPV) and drywell were used as the pressure boundary in this experiment. The RPV was used as the upstream stagnation reservoir and the drywell was used as the downstream receiver with the horizontal test section connecting the RPV and the drywell. The inner diameter of the test section was 2.54cm except at the choking section (nozzle and orifice). Figure 1 shows the schematic of the experimental facility.

**[Figure 1 here]**

Experimental upstream pressure conditions were 0.207MPa (30psia), 0.345MPa (50psia), 0.517MPa (75psia), 0.689MPa (100psia), and 1.034MPa (150psia). The water flow rate from RPV to the test section was determined by the RPV pressure. The drywell was maintained at atmospheric pressure. A steady RPV pressure was maintained by a compressed air supply line that was connected to the top of RPV and was controlled by a regulator. This injection line included a vortex flow meter, a check valve, a needle valve, five ball valves, and two pressure regulators. The air gas flow rate was measured using a vortex flow meter. The injected gas flow rate was controlled by a needle valve. Maximum compressed air pressure of laboratory supply was 1.067MPa. Hence, a compressed nitrogen cylinder (15.27MPa) was used for 1.086MPa supply pressure condition. The compressed air was injected to the horizontal test section through the sparger system. The air injection port was connected to the horizontal test section that was located downstream of the first magnetic flow meter. The sparging system was made of a porous stainless steel tube. The porous tube pore size was 20μm and the length of the sparger was 15.24cm. The sparger inner diameter was 2.54cm. Figure 2 shows the schematic of the air injection port.

**[Figure 2 here]**

The injection port contained a cavity with two air injection ports between the outer surface of the porous element and inner surface of outer cylinder. The pressure drop across the porous tube supplied by the company was about 137.9Pa, for typical flow condition of the tests.

Two types of the break geometry were used, a nozzle and an orifice. Both were made of stainless steel. The throat diameter of the nozzle was 0.54cm and the length of the converging section of the nozzle was 1.08cm with L/D ratio of 2. The orifice throat diameter was the same as the nozzle diameter. The thickness of the orifice plate was 0.3175cm. The orifice throat had a straight cut up to the half of the plate thickness and the remaining half

part had a diverging section with 45 degree. For both nozzle and orifice, a pressure tap was placed at the throat to measure the pressure near the choking section. Another pressure tap was placed at the downstream of the throat to insert a thermocouple for measuring the temperature. Both ends of the nozzle and the orifice were welded with stainless steel tubing of 2.54cm inner diameter with steel flanges. Thermocouple and pressure taps were installed at 2.54cm from upstream and downstream of the flange. The details of the geometry are shown in Figures 3 and 4.

**[Figure 3 here]**

**[Figure 4 here]**

The liquid flow rate was measured with the magnetic flow meter. A check valve was installed at the downstream of the vortex flow meter to avoid the reverse flow of liquid toward the vortex flow meter.

Two impedance meters were used to measure local cross-section averaged void fractions [35]. The impedance meter of 2.54cm inner diameter is composed of two stainless steel rings and three Teflon rings. The two stainless steel rings form the electrodes, and Teflon serves as the insulating material. The impedance signal of this meter is affected by the temperature and the conductivity of the water. Hence, the impedance meter was calibrated for each experimental condition. To calibrate the impedance meter, the voltage signal was measured with empty and full of water. These two values were used as the minimum and maximum value. The empty case corresponded to the void fraction 1 and the full water condition corresponded to the void fraction 0. During the experiment, range of the output voltage signals was set between these two values, and the void fraction was obtained from the calibration curve which was developed separately in a calibration loop.

The pressure, temperature, and flow rate data were collected using a PC based data acquisition system.

Tables 1 and 2 show the test matrix for air-water and subcooled water choking flow test.

**[Table 1 here]**

**[Table 2 here]**

## 4. SLIP RATIO CALCULATION

The main measurement parameters in this study were the slip ratio and the critical flow rate. The critical flow rate was obtained from the magnetic flow meter and the vortex flow meter. The definition of the slip ratio is given as

$$S = \frac{v_g}{v_f}, \tag{8}$$

where $v_g$ is local gas velocity and $v_f$ is local liquid velocity. $v_f$ is calculated using following relation based on the liquid flow rate.

$$\begin{aligned} &\dot{m}_f = \rho A_t v_{f1} = \rho A_f v_{f2} = \rho A_t (1-\alpha) v_{f2} \\ &\therefore v_{f2} = \frac{v_{f1}}{(1-\alpha)} \end{aligned} \tag{9}$$

Because the liquid is incompressible, the liquid density is assumed as a constant. The gas velocity was obtained using following relation.

$$\begin{aligned} \dot{m}_g &= \rho_{up} A_{up} v_{g1} = \rho_{down} A_g v_{g2} \\ &= \rho_{down} \frac{A_g}{A_t} A_t v_{g2} = \rho_{down} A_t \alpha v_{g2} \\ \therefore v_{g2} &= \left(\frac{\rho_{up}}{\rho_{down}}\right)\left(\frac{A_{up}}{A_t}\right)\frac{v_{g1}}{\alpha} \end{aligned}, \tag{10}$$

where $A_{up}$ is the flow area of the gas injection port. $\rho_{up}$ and $\rho_{down}$ were calculated based on the pressure at gas injection port and just upstream of the choking section.

## 5. RESULTS

### 5.1 Air-Water Experiment

#### 5.1.1 Flow Regime and Void Fraction

Simultaneous measurement of flow quality and void fraction is required to obtain the slip ratio. Two impedance meters were used to measure the void fraction as described in the previous section. Figure 5 shows the typical impedance signals for various flow conditions.

**[Figure 5 here]**

It is recognized that the impedance signal pattern is different depending on the flow regime. As the gas velocity increases, the flow regime changes from bubbly flow to slug flow and from slug flow to annular flow. Both impedance meters were located at the upstream location of the choking plane. Between two impedance meters, a magnetic flow meter was located. Therefore, IMP1 (location 2) corresponds to location upstream of the magnetic flow meter and IMP2 (location 3) corresponds to location downstream of the magnetic flow meter. The impedance meter signal is used to measure the slug propagation velocity. It is seen that there is a time difference in corresponding slug signals from IMP1 and IMP2. The distance between two impedance meters divided by time difference between consecutive slug signals gives the slug propagation velocity.

Void fraction for nozzle and orifice geometry is shown in figure 6. The void fraction was obtained by averaging impedance value versus time and using the correlation between the impedance and void fraction [35]. As shown in figures, the void fraction value is almost same at both locations; this is consistent as this result is for air-water case.

**[Figure 6 here]**

5.1.2 Slip Ratio

The key parameter to estimate mechanical non-equilibrium is the slip ratio. If the slip ratio is unity, then the flow is homogeneous. If the slip ratio is larger than unity, then that indicates the degree of the mechanical non-equilibrium.

Figures 7 and 8 show slip ratio as function of quality for nozzle and orifice at various pressures. From figures 7 and 8, it is observed that the slip ratio is higher at low pressure than at high pressure for the same quality. The relationship between void fraction, quality, and slip ratio by definition is given as

$$S = \frac{x}{1-x}\frac{\rho_f}{\rho_g}\frac{1-\alpha}{\alpha} \tag{4}$$

Slip ratio is affected by the density ratio (the ratio of liquid density to gas density).

**[Figure 7 here]**

**[Figure 8 here]**

The density ratio at high pressure is smaller than that at low pressure because the gas density increases with pressure. Therefore, the slip ratio at low pressure is larger than that at high pressure.

Often in literature a constant slip ratio is used which is based on the density ratio to obtain the relationship between quality and void fraction. Moody model [24] and Fauske model [25] defined the slip ratio at the choking cross-section and it only depended on the choking pressure. These models also assumed that the choking pressure is dependent on the upstream pressure. Therefore, the slip ratio cannot reflect the effect of other parameters when the choking pressure is pre-determined. The present study showed that the slip ratio is not only the function of pressure, but also function of the flow quality. This implies that the

mechanical non-equilibrium depends on the pressure, quality, and void fraction. Hence, it is not reasonable to use constant slip ratio.

Figures 9(a) and 9(b) show the break geometry effect on slip ratio at 0.207MPa and 1.034MPa pressure condition. From these figures it is seen that the slip ratio is not affected by the break geometry. However, the measurement location was not at the choking region but at upstream of the choking plane. The break geometry may affect the slip at the choking plane. The errors on slip ratio and flow quality measurements are shown in these figures. The error for slip ratio is 6.36% and the error for flow quality is 3.58%, respectively.

**[Figure 9 here]**

5.1.3 Choking Mass Flux

Figures 10(a)-(e) show the choking mass flux as a function of quality for break geometries for each RPV pressure. The choking mass flux for the nozzle is higher than that for the orifice in the low quality region. The difference in the choking mass flux between orifice and nozzle is smaller at higher quality. This means that there is a geometry effect on choking mass flux in the low quality region, even though there is no difference in the slip ratio at the upstream of choking plane. Therefore, it can be concluded that there may be a mechanical non-equilibrium associated with flow at the choking plane. Since the nozzle has the smooth area change and the orifice has the abrupt area change, the fluid acceleration in the orifice is higher than in the nozzle. This acceleration occurs at the entrance of the choking plane. Hence, it results in higher choking mass flux for the nozzle. In general discharge coefficient for the orifice reduces flow rate. This trend is also similar in the two-phase flow. However, it is difficult to separate the combined effects of the slip ratio and reduced area in the choking mass flux.

**[Figure 10 here]**

## 5.2 Subcooled Water Experiment

Subcooled water experiments were performed to investigate the effect of mechanical and thermal non-equilibrium on the choking flow. The nozzle and the orifice were used to investigate the effect of the geometry on the non-equilibrium effects. The subcooled water choking mass flux is affected by the pressure difference between the upstream and the choking pressure, subcooling, and choking section geometry. Figures 11 and 12 show the measured choking mass flux at different pressures and subcooling for nozzle and orifice, respectively.

**[Figure 11 here]**

**[Figure 12 here]**

The choking pressure at the choking point primarily depends on the upstream pressure and the thermodynamic state at the inlet. If the upstream pressure increases, the choking pressure also increases. The pressure difference between those two pressures mainly determines the choking mass flux, as shown in Figures 11 and 12. There is a large decrease in the pressure across the choking plane. This implies that significant flashing can occur in the immediate upstream and downstream sections of the choking plane. However, it was impossible to find the flashing incipient point. Impedance meter measurements showed no significant flashing of the liquid up to the choking plane. This means that there is no significant phase change at the upstream and the subcooled inlet condition is preserved. The choking mass flux decreases only moderately with subcooling. This means that there is a relatively small effect of the degree of flashing in choking phenomena because for the subcooled water blow down, the thermal non-equilibrium is dominant. Figure 13 shows comparison of the choking mass fluxes for the nozzle and for orifice cases for the 207kPa and 1034kPa operating pressures.

**[Figure 13 here]**

The choking mass flux for the nozzle is slightly higher than for the orifice case. This trend is similar to the air-water case where only mechanical non-equilibrium affects choking flow. This indicates that the mechanical non-equilibrium can affect the subcooled water choking flow. The thermal non-equilibrium effect on choking mass flux exists as shown in Figures 11 and 12. However, it is not much affected by the degree of subcooling except at very small subcooling. In general, if the thermal equilibrium effect is assumed, the flow rate in the orifice is higher than in the nozzle because there is more flashing in nozzle. Therefore, it can be concluded that both mechanical and thermal non-equilibrium are involved in the inlet subcooled water choking flow.

## 6. CONCLUSIONS

Choking flow data for air-water, subcooled water, saturated water and steam-water at low pressures (207kPa to 1034kPa) were obtained for orifice and nozzle geometry. The impedance meter was used to measure the local area averaged void fraction, and to identify the flow regime at upstream of the choking plane. Slip ratio was obtained from data taken with in-line instrumentations such as the impedance meter, magnetic flow meter, and pressure transducer and the thermocouples.

The results of the air-water experiment show that the mechanical non-equilibrium has strong effect on the choking flow at low pressure due to the large density ratio between the liquid and gas which tends to create significant non-equilibrium in accelerating flow. The choking mass flux is affected by the choking section geometry at low quality. It is concluded that there is significant mechanical non-equilibrium at the choking plane even though the slip ratio is identical at the upstream region for air-water choking flow for the nozzle and orifice cases.

The subcooled water experiments were performed to investigate the thermal non-equilibrium effect in addition to the mechanical non-equilibrium effect on choking flow. The experimental data showed that choking flow rate moderately decreases with decrease in subcooling, whereas the code predictions show large decrease in choking flow rate with subcooling. Experimental data indicated that there is a thermal non-equilibrium in the flow and hence the flow rate does not decrease as rapidly with decrease in subcooling. Data comparison between nozzle and orifice showed that for the same subcooling the nozzle choking flow rate is slightly higher than the orifice choking flow rate due to the mechanical non-equilibrium. It was found that the mechanical and thermal non-equilibrium are dominant in subcooled water choking flow.

**ACKNOWLEDGMENTS**

This work was performed under the auspices of the U.S. Nuclear Regulatory Commission.

**NOMENCLATURE**

| | |
|---|---|
| $A$ | Area |
| c | Specific heat |
| $c_p$ | Specific heat |
| D | Diameter |
| G | Mass flux ($kg/m^2s$) |
| $h$ | Enthalpy |
| L | Length |
| $\dot{m}$ | Mass flow rate |
| N | Experimental parameter |
| n | Polytropic exponent |
| P | Pressure |
| s | Entropy |
| $S$ | Slip Ratio |
| T | Temperature |
| $v$ | Specific volume |
| V | Velocity |
| $x$ | Quality |

Greek Letters

| | |
|---|---|
| $\alpha$ | Void Fraction |
| $\gamma$ | Isentropic exponent |
| $\eta$ | Pressure ratio |
| $\rho$ | Density |
| $\omega$ | Correlating parameter |

Superscripts

| | |
|---|---|
| * | Nomalized value |

Subscripts

| | |
|---|---|
| c | Choking |
| down | Downstream |
| E | Equilibrium |

| | |
|---|---|
| *f* | Liquid |
| *g* | Vapor or gas phase |
| m | Mixture |
| o | Stagnation |
| s | Saturation |
| sub | Subcooling |
| t | Total |
| up | Upstream |

**REFERENCE**


1. Schrock, V.E., Amos, C.A., Two-phase Flow and Heat Transfer, China-U.S. Seminar on Two-Phase Flows and Heat Transfer, Sian, China, 1984, pp 115-138.
2. Sauvage, Ecoulement de L'eau des Chaudieres, Annales des Mines, 9, Vol. II, 1892.
3. Rateau, A., Experimental Researches on the Flow of Steam through Nozzles and Orifice, to which is added a Note on the Flow of Hot Water, A. Constable and Co., Ltd, London, 1905.
4. Starkman, E.S., Schrock, V.E., Neusen, K.F., Maneely, D.J., Expansion of a Very Low Quality Two-Phase Fluid through a Convergent-Divergent Nozzle, Journal of Basic Engineering, TRANS. ASME, Series D, Vol. 86, No 2, June 1964, pp. 247-256.W. Wulff et al., Quantifying Reactor Safety Margins, Part 3: Assessment and Ranging of Parameters, Nuclear Engineering and Design, Vol.119, 33-65, 1990
5. Wallis, G.B., Critical Two-Phase Flow, Int. J. Multiphase Flow, Vol. 6, pp. 97-112, 1980.
6. Abdollahian, D., Healzer, J., Janssen, E., Amos, C., Critical Flow Data Review and Analysis, Final Report, S. Levy, Inc. EPRI Report NP-2192, 1982.
7. Fthenakis, V.M., Rohatgi, U.S., Chung, B.D., A Simple Model for Predicting the Release of a Liquid-Vapor Mixture from a Large Break in a Pressurized Container, Journal of loss Prevention in the Process Industries 16, pp. 61-72, 2003.
8. Darby, R., Perspectives on Relief Valves Sizing for Two-phase Flow, International Symposium on Runaway Reactions, Pressure Relief Design, and Effluent Handling, Mach 11-13, New Orleans, Louisiana, pp. 365-397, 1998.
9. Epstein, M., Henry, R.E., Midvidy, W., Pauls, R., One-dimensional Modeling of Two-phase Jet Expansion and Impingement, Thermal-Hydraulics of Nuclear Reactors II, 2nd Int. Topical Meeting on Nuclear Reactor Thermal-Hydraulics, Santa Barbara, CA, 1983.

10. Leung, J.C., A Generalized Correlation for One-component Homogeneous Equilibrium Flashing Choked Flow; AIChE J., Vol. 32, pp. 1743-1746, 1986.
11. Leung, J.C., Grolme, M.A., A Generalized Correlation for Flashing Choked Flow of Initially Subcooled Liquid, AIChE J., Vol. 34, No. 4, pp. 688-691, 1986.
12. Saha, P., A Review of Two-Phase Steam-Water Critical Flow Models with Emphasis on Thermal Non-equilibrium, BNL-NUREG-50907, 1978.
13. A group of expert of the NEA Committee on the Safety of Nuclear Installations, Critical Flow Modeling in Nuclear Safety, Nuclear Energy Agency, June, 1982.
14. Khajehnajafi, S., Shinde, A., Prediction of Discharge Rate from Pressurized Vessel Blowdown through Sheared Pipe, Process Safety Progress, Vol. 14, No. 1, pp. 22-25, 1995.
15. Schrock, V.E., Starkman, E.S., Brown, R.A., Flashing Flow of Initially Subcooled Water in Convergent-Divergent Nozzle, Trans. ASME, J. Heat Transfer 99, pp. 263-268, 1977.
16. Henry R.E., Fauske, H.K., The Two-Phase Critical Flow of One Composition Mixtures in Nozzle, Orifices, and Short Tubes, J. Heat Transfer 93, pp. 179-187, 1971.
17. Schultz, R. R., Ericson, L., "The Marviken Critical Flow Test Program," Nuclear Safety, Vol. 22, No. 6, pp. 712-724, 1981.
18. Levy, S., Abdollahian, D., Homogeneous Non-equilibrium Critical Flow Model, Int. J. Heat Mass Transfer, Vol. 25, No 6, pp. 759-770, 1982.
19. Reocreux, M., Contribution à létude des debits critiques en enoulement diphasique eau-vapeur, Ph.D. thesis, Lúniversité Scientifique et médicale de Grenoble, 1974.
20. Zimmer, G.A., Wu, B.J.C., Leonhardt, W.J., Abuaf, N., Jones, O.C., Pressure and Void Distributions in a Conversing-Diverging Nozzle with Non-equilibrium Water Vapor Generation, BNL-NUREG-26003, 1979.

21. Fincke, J.R., Collons, D.R., The Correlation of Two-dimensional and Nonequilibrium Effects in Subcooled Choked Nozzle Flow, NUREG/CR-1907, EGG-2081, 1981.

22. Sozzi, G. L., Sutherland, W. A., "Critical Flow of Saturated and Subcooled Water at High Pressure," General Electric Report NEDO-13418, 1975

23. Lenzing, T., Friedel, L., Cremers, J., Alhusein, M., Prediction of the Maximum Full Lift Safety Valve Two-phase Flow Capacity, Journal of Loss Prevension in the Process Industries, Vol. 11, pp. 307-321, 1998.

24. Moody, F.J., Maximum Flow Rate of a Single Component, Two-Phase Mixture, Trans. ASME, J. Heat Transfer 86, pp.134-142, 1965.

25. Fauske, H.K., Two-Phase Critical Flow with Application to Liquid Metal System, ANL-6633, 1963.

26. Fauske, H.K., Contribution to the theory of two-phase, one-component critical flow, Ph.D Thesis, 1962

27. Lottes, P.A., Petrick, M., Marchaterre, J.F., Lecture Notes on Heat Extraction from Boiling Water Power Reactors, Presented at the Advanced Summer Institute at Kjeller, Norway, August 17-29, ANL-6063, 1959.

28. Cruver, J.E., Moulton, R.W., Critical Flow of Liquid Vapor Mixture, AIChE J. Vol. 13, No. 1, pp. 52-60, 1967.

29. Bouré, J.A., Two-Phase Flows with Application to Nuclear Reactor Design Problem, von Karman Institute for Fluid Dynamics, Lecture Series, Grenoble, France, 1974.

30. Ishii, M., One-dimensional drift-flux model and constitutive equations for relative motion between phases in various two-phase flow regimes, ANL-77-47, 1977.

31. Ransom, V.H., Trapp, J.A., " The RELAP5 Choked Flow Model and Application to a Large Scale Flow Test," Proceeding of the ANS/ASME/NRC International Topical

Meeting on Nuclear Reactor Thermal-Hydraulics, Saratoga Springs, New York, October 5-8, pp.799-819, 1980.

32. Richter, H.J., Separated Two-Phase Flow Model: Application to Critical Two-Phase Flow, Int. J. Multiphase Flow, Vol. 9, No. 5, pp. 511-530, 1983.
33. GE nuclear Energy, SBWR Standard Safety Analysis Report, Report No. 25A5113 Rev. A 1992.
34. Ishii, M., Revankar, S.T., Leonardi, T., Dowlati, R., Bertodano, M.L., Babelli, I., Wang, W., Pokharna, H., Ransom, V.H., Viskanta, R., Han, J.T., Scientific Design of Purdue University Multi-Dimensional Integral Test Assembly (PUMA) for GE SBWR, Purdue University Report PU-NE-94/1, U.S. Nuclear Regulatory Commission Report NUREG/CR-6309, 1996.
35. Revankar, S.T., Ishii, M., Mi, Y., Bertodano, M.L., Xu, Y., Kelly, S., Ransom, V.H., Han, J.T., "Instrumentation for the PUMA Integral Test Facility," NUREG/CR-5578, 1998.

LIST OF FIGURES

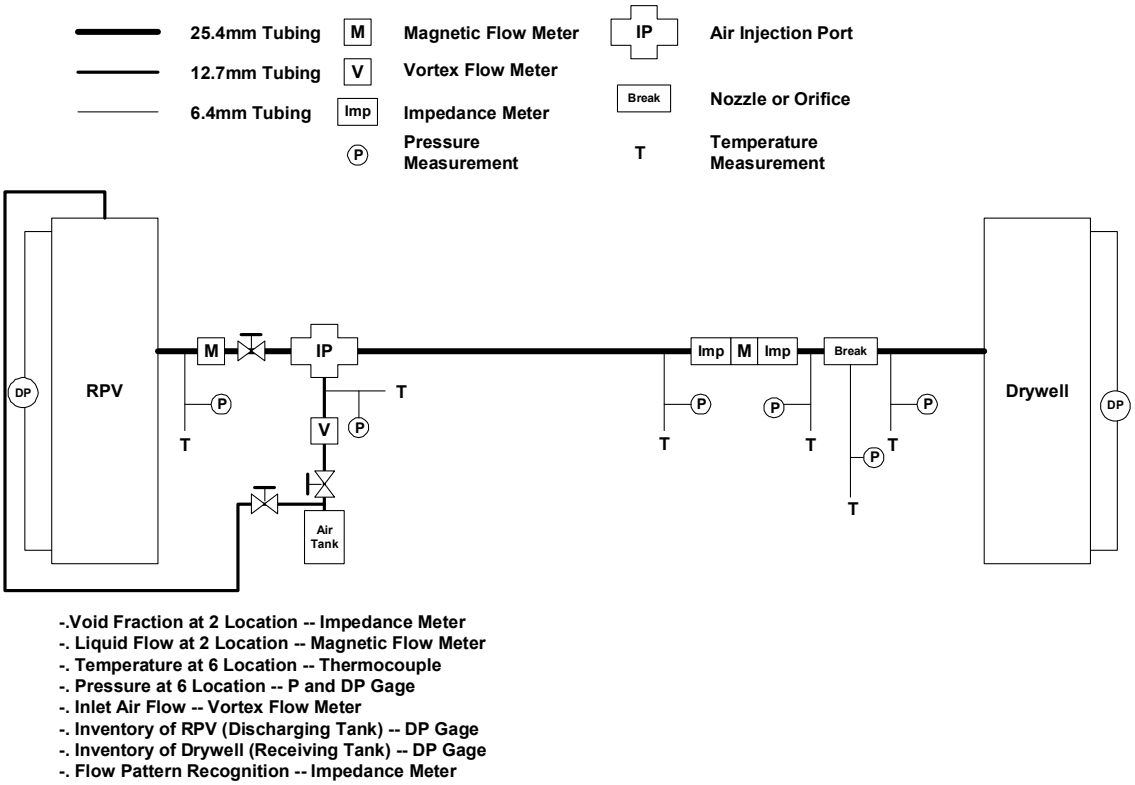


Figure 1 Schematic Diagram of Experimental Facility

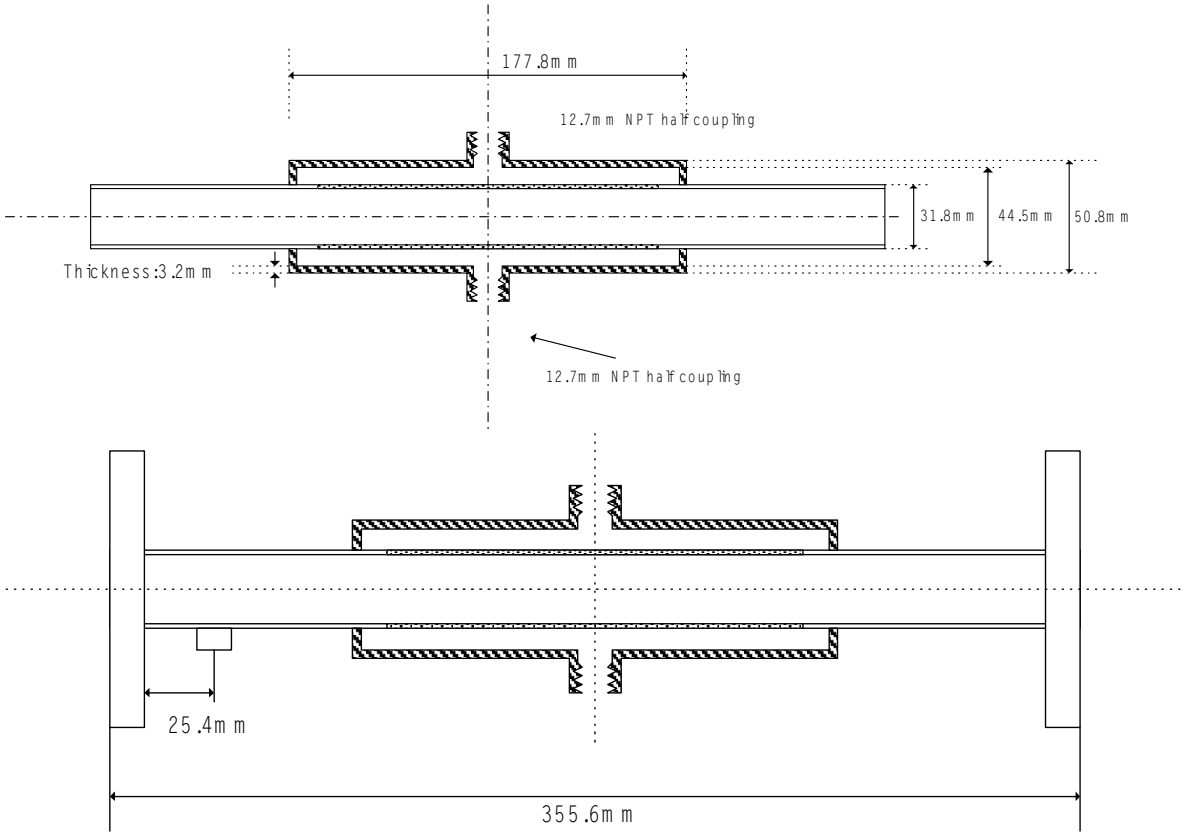


Figure 2 Air Injection Port

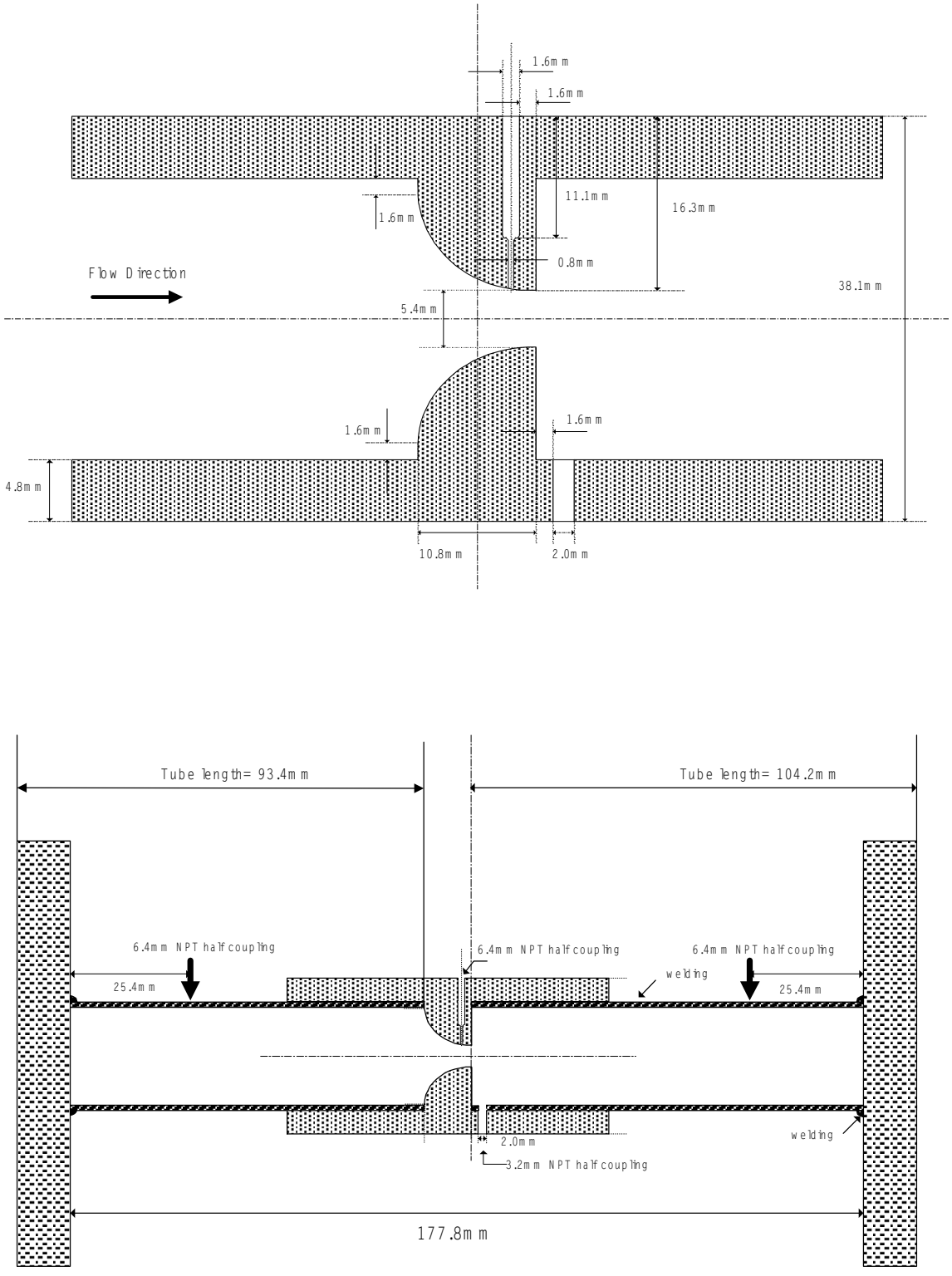


Figure 3 Test Section—Nozzle

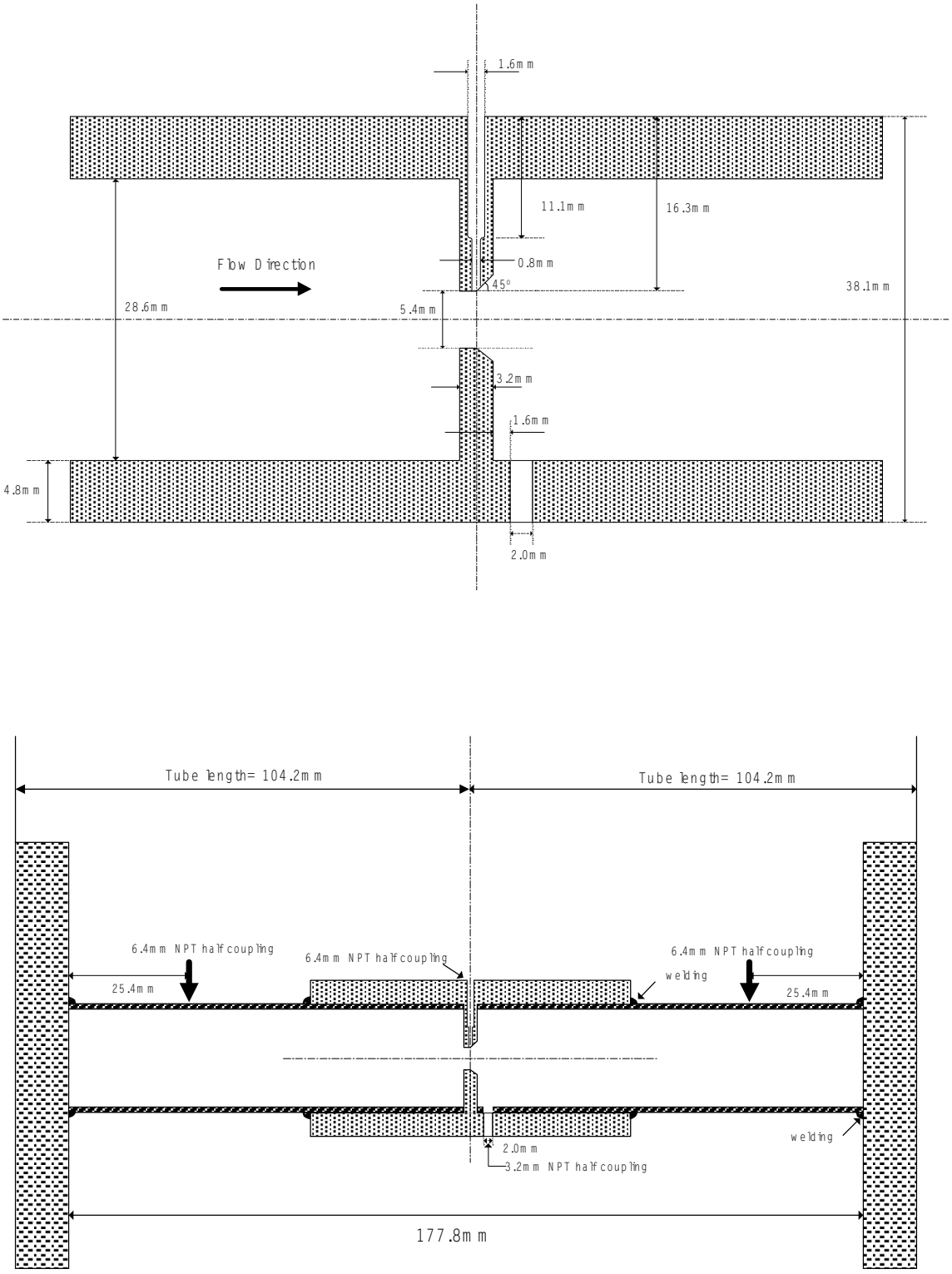


Figure 4 Test Section—Orifice

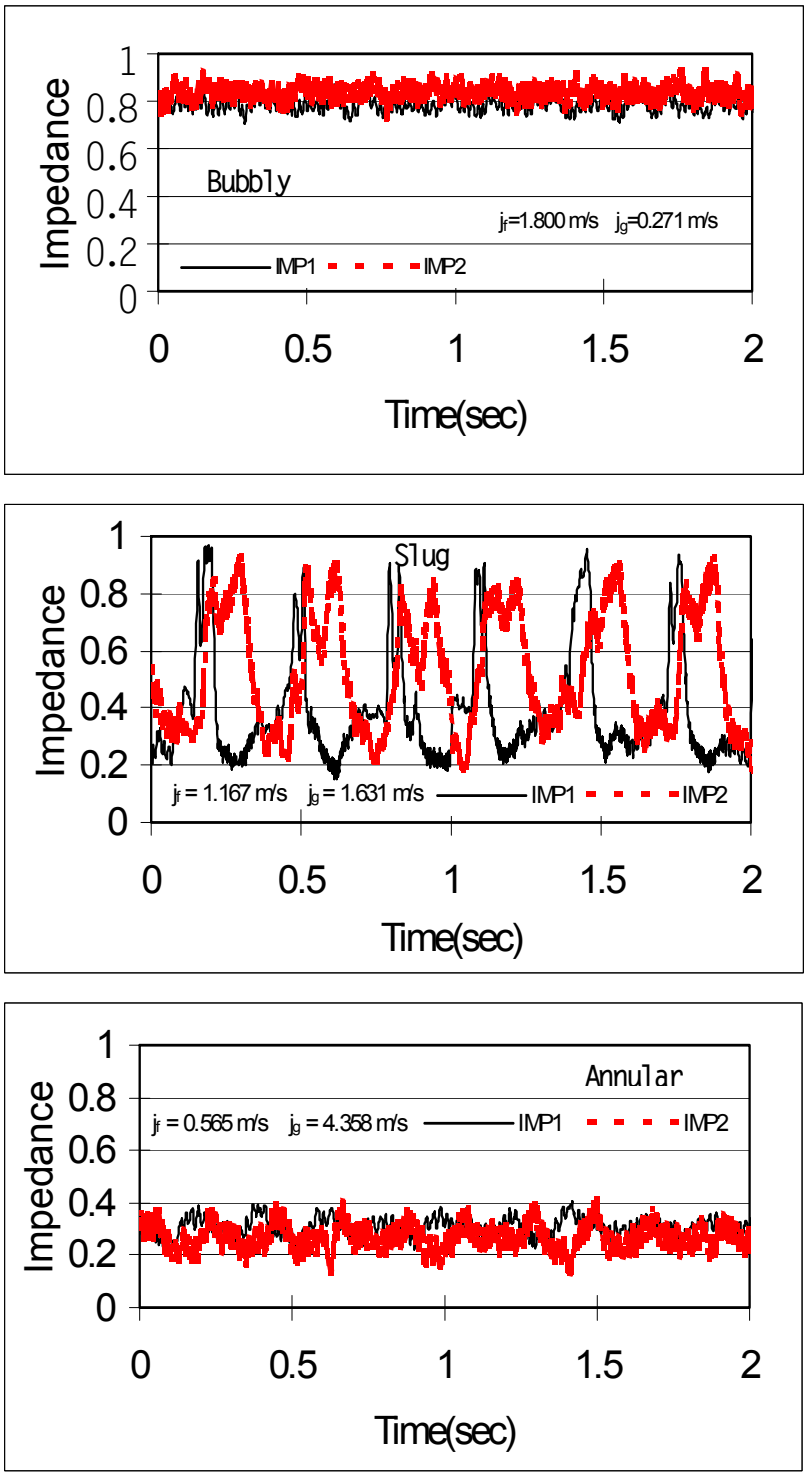


Figure 5 Flow Regime Identification Using Impedance Meter Signal

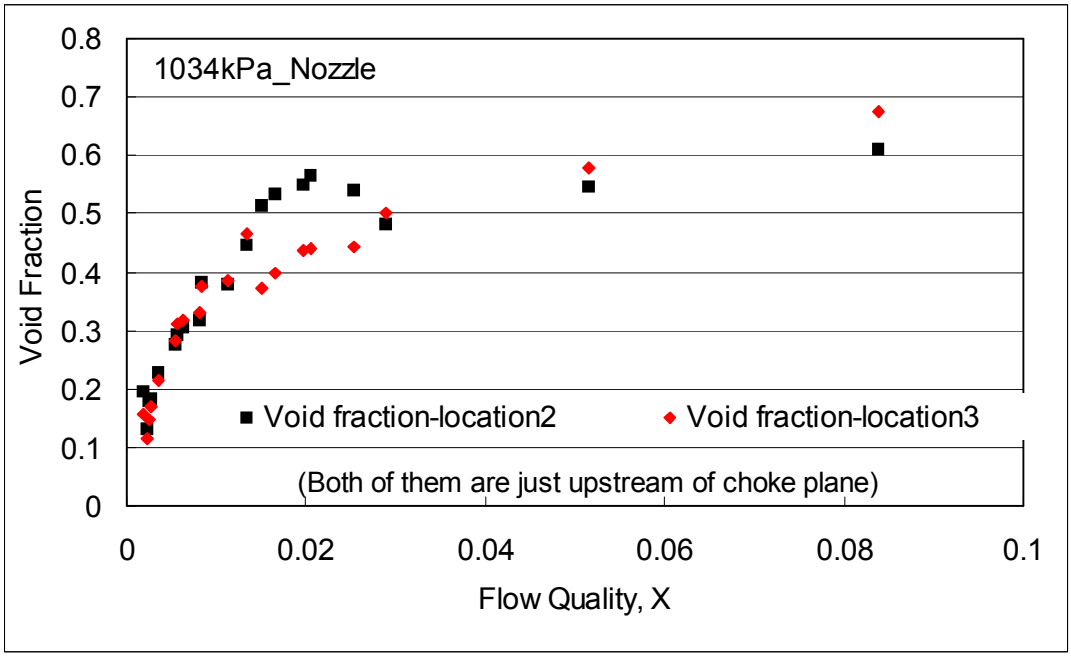


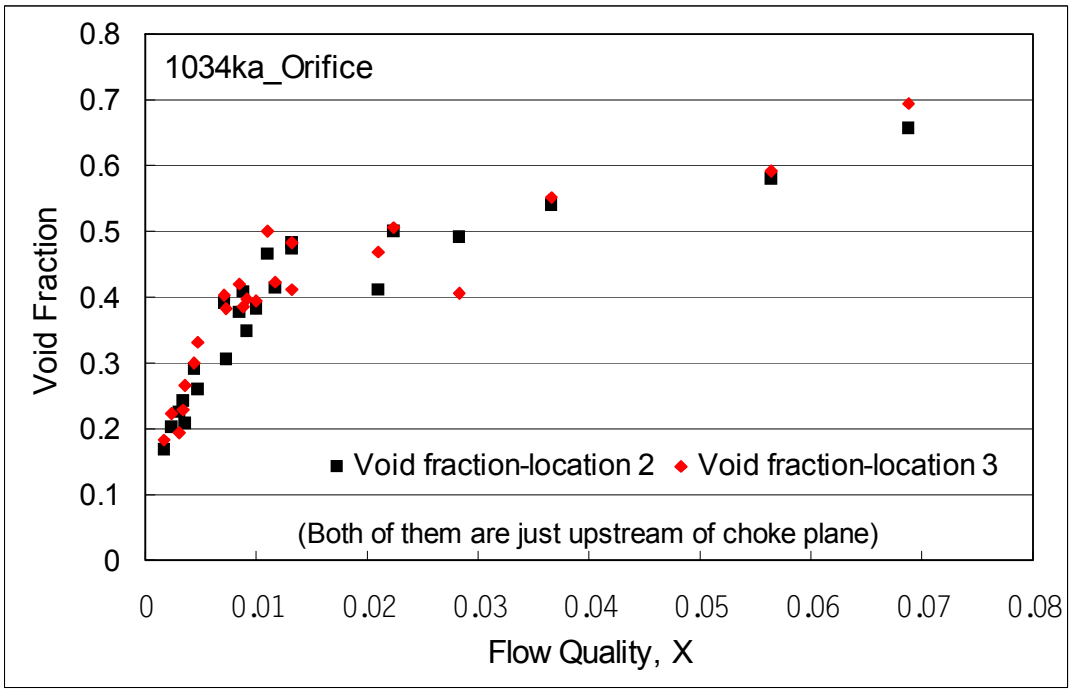


Figure 6 Void Fraction VS Quality

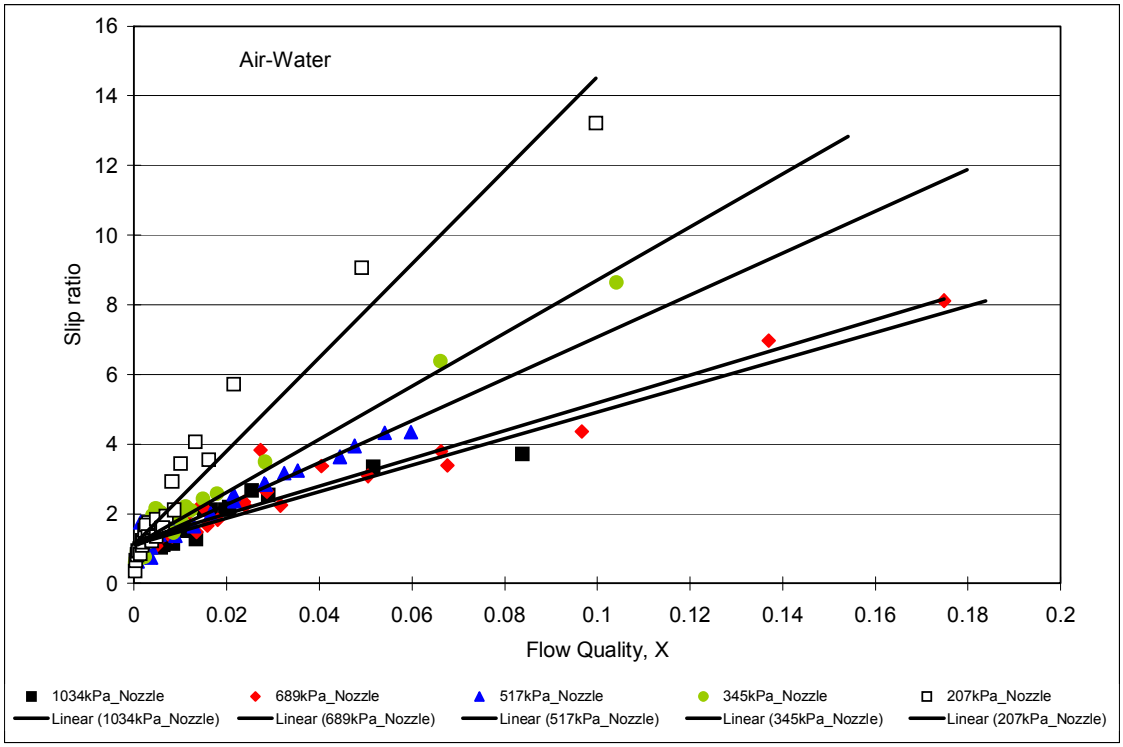


Figure 7 Pressure Effect on Slip Ration in Nozzle (Air-Water)

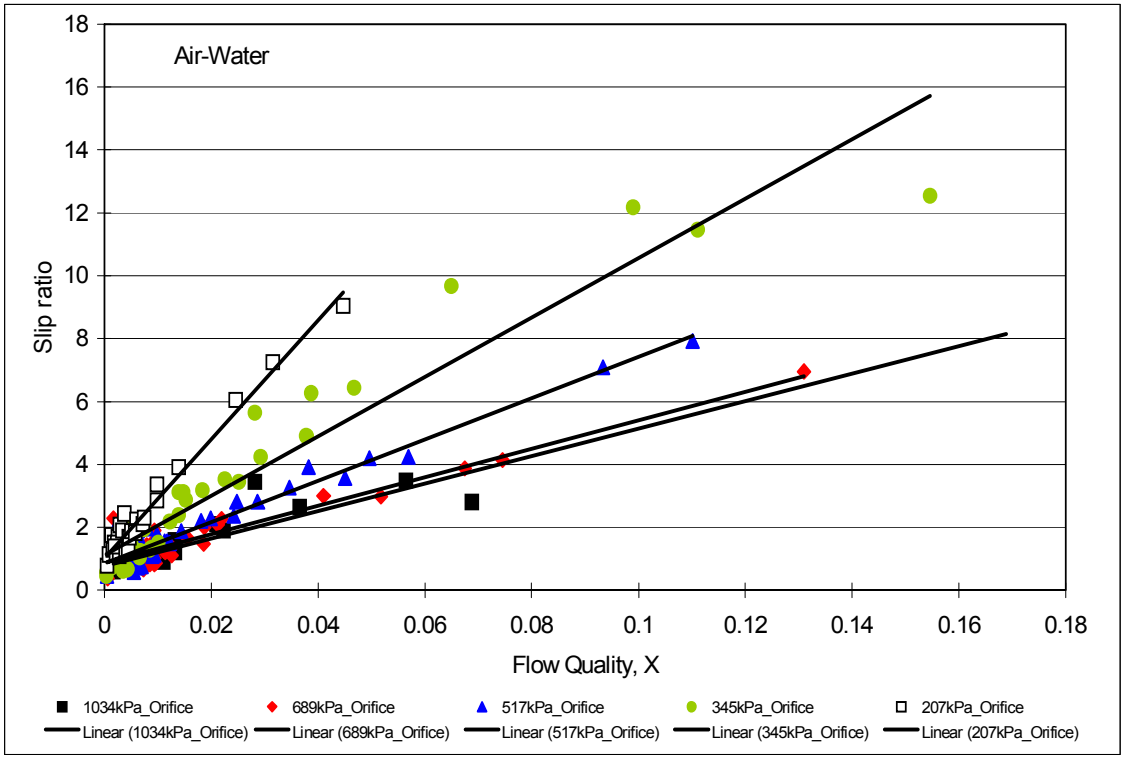


Figure 8 Pressure Effect on Slip Ratio in Orifice (air-Water)

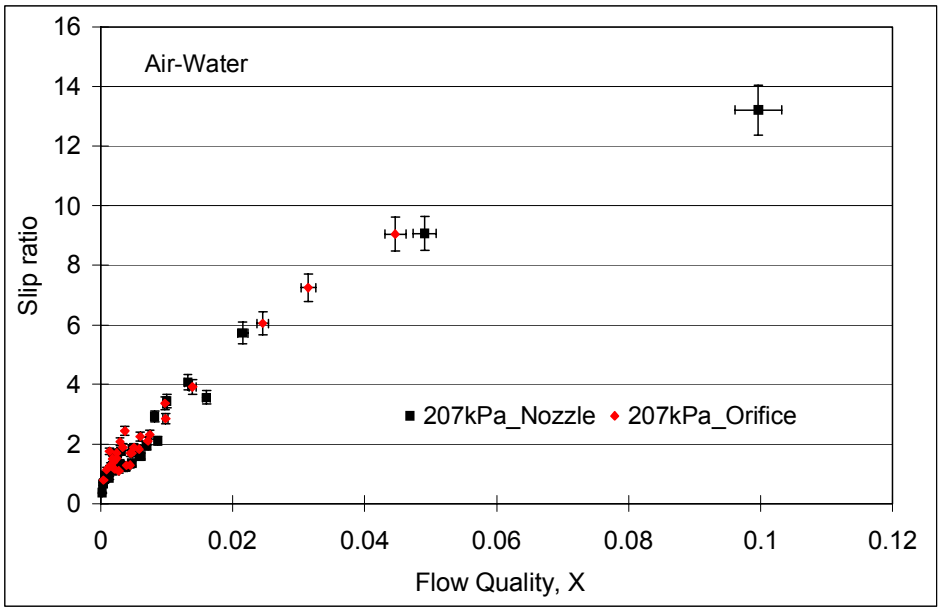


(a) 207 kPa

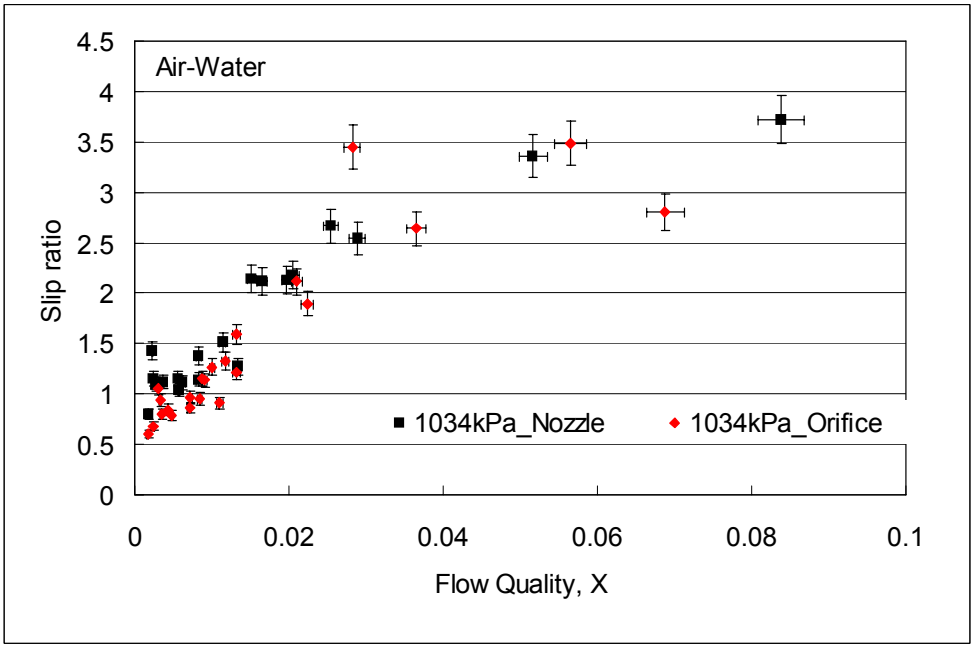


(b) 1034kPa

Figure 9 Slip Ratio Comparisons between Nozzle and Orifice

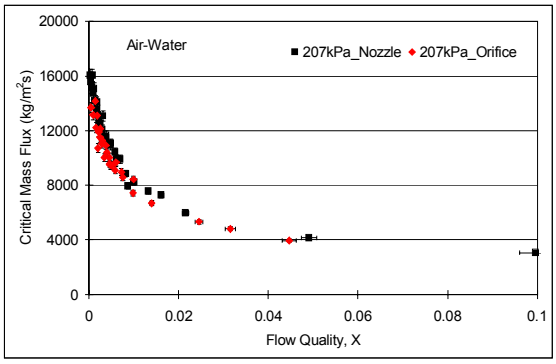


(a) 207 kPa

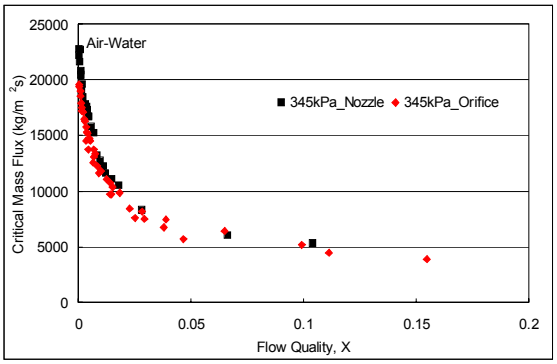


(b) 345 kPa

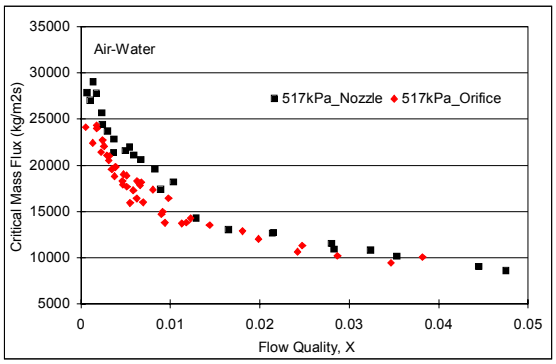


(c) 517 kPa

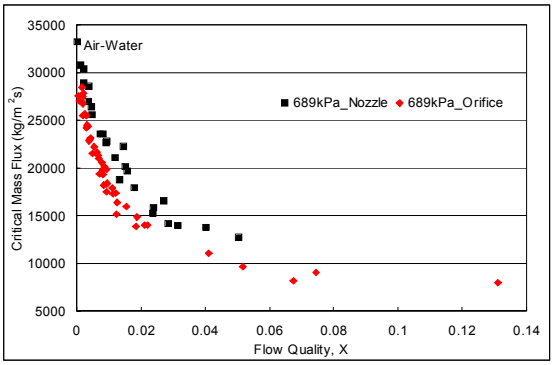


(d) 689 kPa

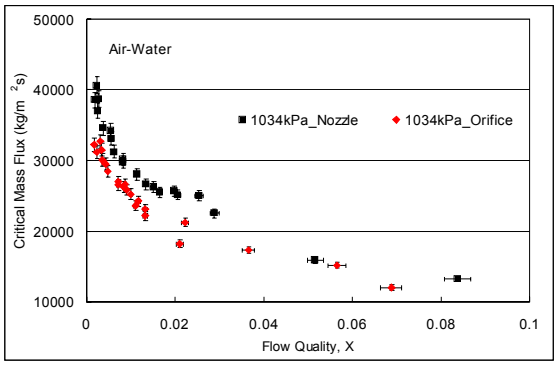


(e) 1034 kPa

Figure 10 Choking Mass Flux for Each Pressure

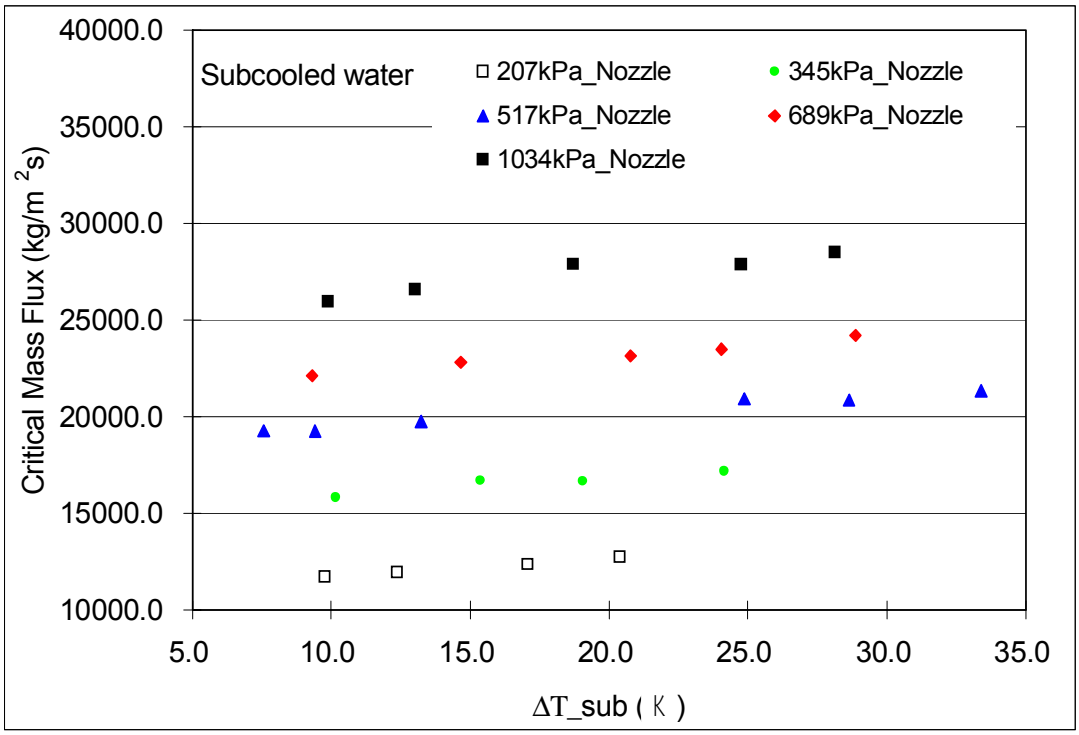


Figure 11 Effect of Pressure on Nozzle (Subcooled Water)

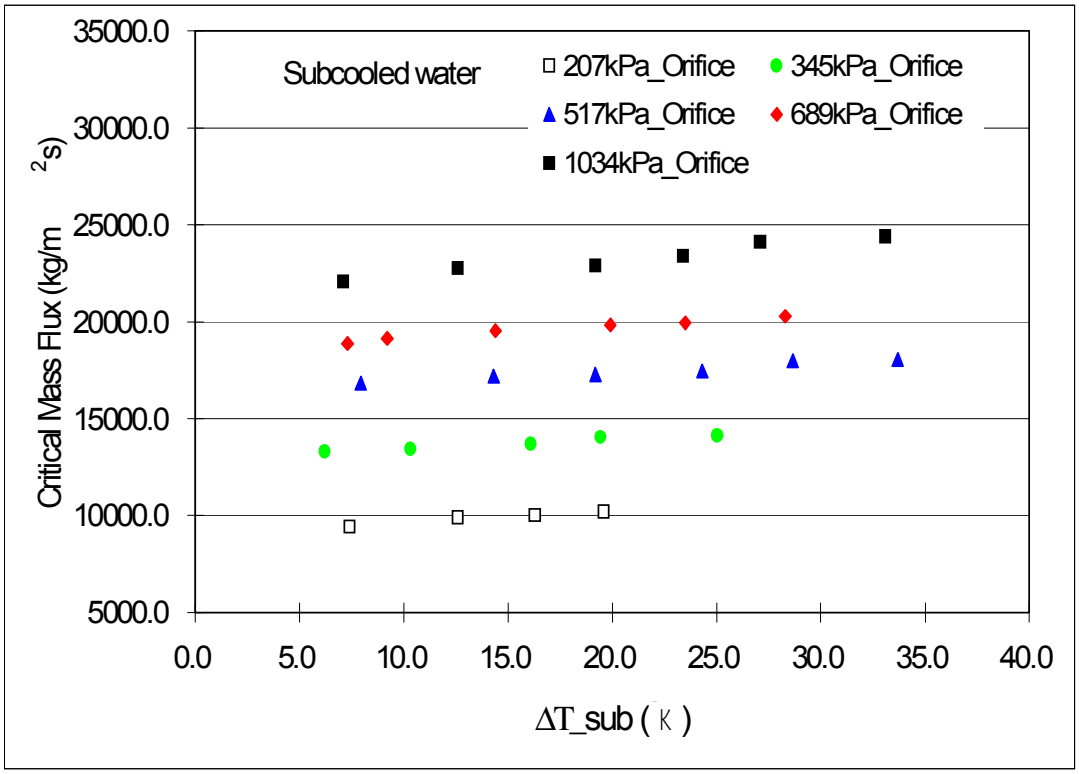


Figure 12 Effect of Pressure on Orifice (Subcooled Water)

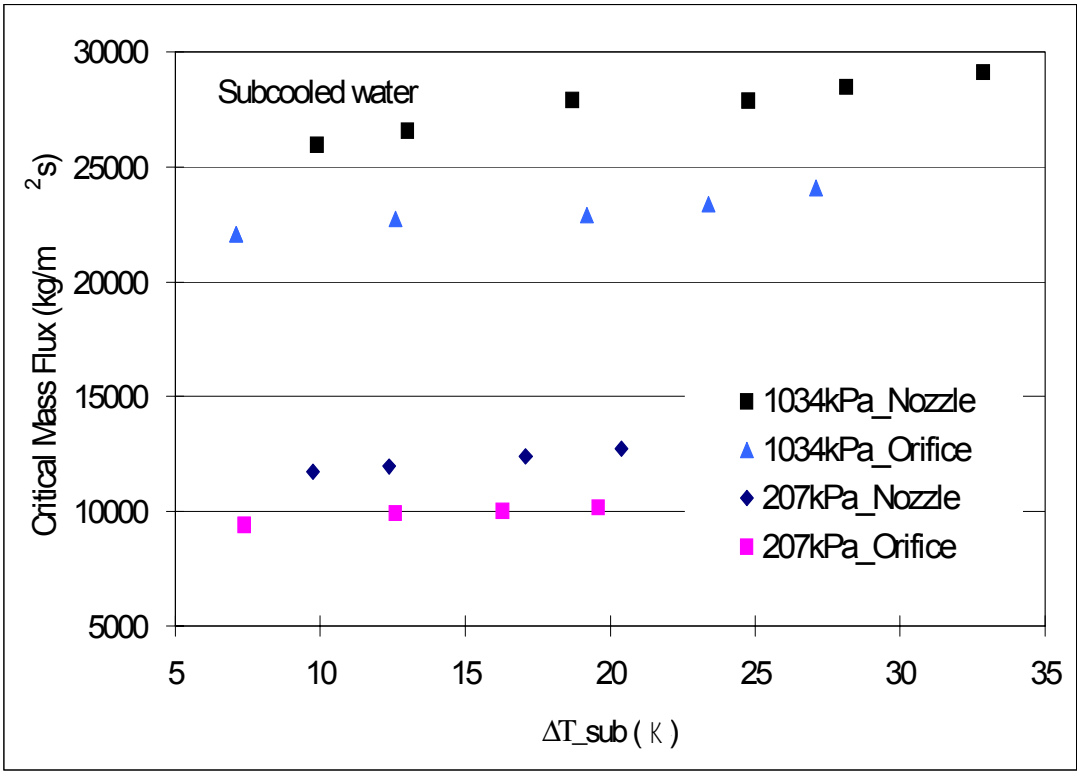


Figure 13 Geometry Effect on 207kPa and 1034kPa (Subcooled Water)

LIST OF TABLES

Table 1 Air-Water Test Matrix
(Mechanical Non-equilibrium Assessment)

| RPV Pressure (kPa) | Choking Section Geometry | Liquid Mass Flow Rate (kg/s) | Air Mass Flow Rate $x10^3$ (kg/s) | Inlet Flow Quality $x10^3$ | Void Fraction (%) |
|---|---|---|---|---|---|
| 207 | Nozzle | 0.063~0.368 | 0.095~6.977 | 0.03~10.0 | 11.4~78.2 |
| | Orifice | 0.086~0.324 | 0.143~4.035 | 0.05~4.5 | 12.3~69.1 |
| 345 | Nozzle | 0.109~0.521 | 0.136~12.709 | 0.03~10.4 | 8.6~77.0 |
| | Orifice | 0.745~0.447 | 0.153~13.679 | 0.03~15.5 | 10.1~79.7 |
| 517 | Nozzle | 0.155~0.663 | 0.464~9.841 | 0.07~6.0 | 11.3~71.2 |
| | Orifice | 0.139~0.556 | 0.296~17.195 | 0.05~11.0 | 11.4~72.4 |
| 689 | Nozzle | 0.180~0.760 | 0.354~35.112 | 0.05~17.5 | 7.1~76.7 |
| | Orifice | 0.159~0.651 | 0.425~23.973 | 0.07~13.2 | 8.5~75.2 |
| 1034 | Nozzle | 0.277~0.928 | 1.608~25.337 | 0.18~8.4 | 11.7~67.5 |
| | Orifice | 0.256~0.746 | 1.231~19.600 | 0.17~6.9 | 16.8~69.4 |

Table 2 Subcooled Water Test Matrix
(Thermal Non-equilibrium Assessment)

| RPV Pressure (kPa) | Choking Section Geometry | Liquid Mass Flow Rate (kg/s) | $\Delta T_{sub}$ (K) |
|---|---|---|---|
| 207 | Nozzle | 0.262~0.285 | 9.8~20.4 |
| | Orifice | 0.210~0.228 | 7.4~20.8 |
| 345 | Nozzle | 0.350~0.389 | 10.2~24.1 |
| | Orifice | 0.298~0.318 | 6.2~25.0 |
| 517 | Nozzle | 0.419~0.469 | 7.6~33.4 |
| | Orifice | 0.377~0.407 | 7.9~33.7 |
| 689 | Nozzle | 0.485~0.544 | 9.3~28.9 |
| | Orifice | 0.420~0.453 | 7.3~28.3 |
| 1034 | Nozzle | 0.560~0.648 | 9.9~32.9 |
| | Orifice | 0.473~0.536 | 7.1~33.1 |